Accurate and agile digital control of optical phase, amplitude and frequency for coherent atomic manipulation of atomic systems

Joseph Thom,[1,2] Guido Wilpers,[1] Erling Riis,[2] and Alastair G. Sinclair[1,*]

[1]*National Physical Laboratory, Teddington, Middlesex, TW11 0LW, UK*
[2]*SUPA, Dept. of Physics, University of Strathclyde, Glasgow, G4 0NG, UK*
[*]*alastair.sinclair@npl.co.uk*

Abstract: We demonstrate a system for fast and agile digital control of laser phase, amplitude and frequency for applications in coherent atomic systems. The full versatility of a direct digital synthesis radiofrequency source is faithfully transferred to laser radiation via acousto-optic modulation. Optical beatnotes are used to measure phase steps up to 2π, which are accurately implemented with a resolution of ≤ 10 mrad. By linearizing the optical modulation process, amplitude-shaped pulses of durations ranging from 500 ns to 500 ms, in excellent agreement with the programmed functional form, are demonstrated. Pulse durations are limited only by the 30 ns rise time of the modulation process, and a measured extinction ratio of $> 5 \times 10^{11}$ is achieved. The system presented here was developed specifically for controlling the quantum state of trapped ions with sequences of multiple laser pulses, including composite and bichromatic pulses. The demonstrated techniques are widely applicable to other atomic systems ranging across quantum information processing, frequency metrology, atom interferometry, and single-photon generation.

OCIS codes: (300.6520) Spectroscopy, trapped ion; (300.6210) Spectroscopy, atomic; (020.1670) Coherent optical effects; (270.5585) Quantum information and processing; (120.0120) Instrumentation, measurement, and metrology.

References and links

1. T. D. Ladd, F. Jelezko, R. Laflamme, Y. Nakamura, C. Monroe, and J. L. O'Brien, "Quantum computers," Nature **464**(7285), 45–53 (2010).
2. H. S. Margolis, "Frequency metrology and clocks," J. Phys. B: At. Mol. Opt. **42**(15), 154017 (2009).
3. A. D. Cronin, J. Schmiedmayer, and D. E. Pritchard, "Optics and interferometry with atoms and molecules," Rev. Mod. Phys. **81**(3), 1051–1129 (2009).
4. C. Roos, T. Zeiger, H. Rohde, H. C. Nägerl, J. Eschner, D. Leibfried, F. Schmidt-Kaler, and R. Blatt, "Quantum state engineering on an optical transition and decoherence in a Paul trap," Phys. Rev. Lett. **83**(23), 4713–4716 (1999).
5. B. B. Blinov, D. Leibfried, C. Monroe, and D. J. Wineland, "Quantum computing with trapped ion hyperfine qubits," Quant. Inform. Process. **3**(1-5), 45–59 (2004).
6. F. Schmidt-Kaler, H. Häffner, M. Riebe, S. Gulde, G. P. T. Lancaster, T. Deuschle, C. Becher, C. F. Roos, J. Eschner, and R. Blatt, "Realization of the Cirac-Zoller controlled-NOT quantum gate," Nature **422**(6930), 408–411 (2003).
7. D. Leibfried, B. DeMarco, V. Meyer, D. Lucas, M. Barrett, J. Britton, W. M. Itano, B. Jelenković, C. Langer, T. Rosenband, and D. J. Wineland, "Experimental demonstration of a robust, high-fidelity geometric two ion-qubit phase gate," Nature **422**(6930), 412–415 (2003).
8. S. Gulde, M. Riebe, G. P. T. Lancaster, C. Becher, J. Eschner, H. Häffner, F. Schmidt-Kaler, I. L. Chuang, and R. Blatt, "Implementation of the Deutsch-Jozsa algorithm on an ion-trap quantum computer," Nature **421**(6918), 48–50 (2003).
9. K.-A. Brickman, P. C. Haljan, P. J. Lee, M. Acton, L. Deslauriers, and C. Monroe, "Implementation of Grover's quantum search algorithm in a scalable system," Phys. Rev. A **72**(5), 050306 (2005).
10. M. Riebe, H. Häffner, C. F. Roos, W. Hänsel, J. Benhelm, G. P. T. Lancaster, T. W. Körber, C. Becher, F. Schmidt-Kaler, D. F. V. James, and R. Blatt, "Deterministic quantum teleportation with atoms," Nature **429**(6993), 734–737 (2004).

#191977 - $15.00 USD Received 10 Jun 2013; revised 19 Jul 2013; accepted 21 Jul 2013; published 30 Jul 2013

11. M. D. Barrett, J. Chiaverini, T. Schaetz, J. Britton, W. M. Itano, J. D. Jost, E. Knill, C. Langer, D. Leibfried, R. Ozeri, and D. J. Wineland, "Deterministic quantum teleportation of atomic qubits," Nature **429**(6993), 737–739 (2004).
12. D. Leibfried, M. D. Barrett, T. Schaetz, J. Britton, J. Chiaverini, W. M. Itano, J. D. Jost, C. Langer, and D. J. Wineland, "Toward Heisenberg-limited spectroscopy with multiparticle entangled states," Science **304**(5676), 1476–1478 (2004).
13. C. F. Roos, M. Chwalla, K. Kim, M. Riebe, and R. Blatt, "'Designer atoms' for quantum metrology," Nature **443**(7109), 316–319 (2006).
14. P. O. Schmidt, T. Rosenband, C. Langer, W. M. Itano, J. C. Bergquist, and D. J. Wineland, "Spectroscopy using quantum logic," Science **309**(5735), 749–752 (2005).
15. C. W. Chou, D. B. Hume, J. C. J. Koelemeij, D. J. Wineland, and T. Rosenband, "Frequency comparison of two high-accuracy Al^+ optical clocks," Phys. Rev. Lett. **104**(7), 070802 (2010).
16. V. Letchumanan, P. Gill, E. Riis, and A. G. Sinclair, "Optical Ramsey spectroscopy of a single trapped $^{88}Sr^+$ ion," Phys. Rev. A **70**(3), 033419 (2004).
17. V. Letchumanan, P. Gill, A. G. Sinclair, and E. Riis, "Optical-clock local-oscillator stabilization scheme," J. Opt. Soc. Am. B **23**(4), 714–717 (2006).
18. N. Huntemann, B. Lipphardt, M. Okhapkin, C. Tamm, E. Peik, A. V. Taichenachev, and V. I. Yudin, "Generalized ramsey excitation scheme with suppressed light shift," Phys. Rev. Lett. **109**(21), 213002 (2012).
19. M. Kasevich and S. Chu, "Laser cooling below a photon recoil with three-level atoms," Phys. Rev. Lett. **69**(12), 1741–1744 (1992).
20. A. Peters, K. Y. Chung, and S. Chu, "High-precision gravity measurements using atom interferometry," Metrologia **38**(1), 25–61 (2001).
21. M. J. Snadden, J. M. McGuirk, P. Bouyer, K. G. Haritos, and M. A. Kasevich, "Measurement of the Earth's gravity gradient with an atom interferometer-based gravity gradiometer," Phys. Rev. Lett. **81**(5), 971–974 (1998).
22. T. L. Gustavson, P. Bouyer, and M. A. Kasevich, "Precision rotation measurements with an atom interferometer gyroscope," Phys. Rev. Lett. **78**(11), 2046–2049 (1997).
23. S.-W. Chiow, T. Kovachy, H.-C. Chien, and M. A. Kasevich, "102$\hbar$k large area atom interferometers," Phys. Rev. Lett. **107**(13), 130403 (2011).
24. S.-W. Chiow, T. Kovachy, J. M. Hogan, and M. A. Kasevich, "Generation of 43 W of quasi-continuous 780 nm laser light via high-efficiency, single-pass frequency doubling in periodically poled lithium niobate crystals," Opt. Lett. **37**(18), 3861–3863 (2012).
25. M. Hijlkema, B. Weber, H. P. Specht, S. C. Webster, A. Kuhn, and G. Rempe, "A single-photon server with just one atom," Nat. Phys. **3**(4), 253–255 (2007).
26. P. B. R. Nisbet-Jones, J. Dilley, A. Holleczek, O. Barter, and A. Kuhn, "Photonic qubits, qutrits and ququads accurately prepared and delivered on demand," New J. Phys. **15**(5), 053007 (2013).
27. M. H. Levitt, "Composite pulses," Prog. Nucl. Mag. Res. Sp. **18**(2), 61–122 (1986).
28. A. Sørensen and K. Mølmer, "Quantum computation with ions in thermal motion," Phys. Rev. Lett. **82**(9), 1971–1974 (1999).
29. J. Benhelm, G. Kirchmair, C. F. Roos, and R. Blatt, "Towards fault-tolerant quantum computing with trapped ions," Nat. Phys. **4**(6), 463–466 (2008).
30. J. Benhelm, G. Kirchmair, C. F. Roos, and R. Blatt, "Experimental quantum-information processing with $^{43}Ca^+$ ions," Phys. Rev. A **77**(6), 062306 (2008).
31. R. Bowler, U. Warring, J. W. Britton, B. C. Sawyer, and J. Amini, "Arbitrary waveform generator for quantum information processing with trapped ions," Rev. Sci. Instrum. **84**(3), 033108 (2013).
32. B. C. Young, F. C. Cruz, W. M. Itano, and J. C. Bergquist, "Visible Lasers with Subhertz Linewidths," Phys. Rev. Lett. **82**(19), 3799–3802 (1999).
33. M. M. Boyd, T. Zelevinsky, A. D. Ludlow, S. M. Foreman, S. Blatt, T. Ido, and J. Ye, "Optical atomic coherence at the 1-second time scale," Science **314**(5804), 1430–1433 (2006).
34. R. Blatt and D. Wineland, "Entangled states of trapped atomic ions," Nature **453**(7198), 1008–1015 (2008).
35. F. Riehle, Th. Kisters, A. Witte, J. Helmcke, and C. J. Bordé, "Optical Ramsey spectroscopy in a rotating frame: Sagnac effect in a matter-wave interferometer," Phys. Rev. Lett. **67**(2), 177–180 (1991).
36. P. Gill, W. Murray, and M. H. Wright, *Practical Optimization* (Emerald, 1982).
37. F. J. Harris, "On the use of windows for harmonic analysis with the discrete Fourier transform," Proc. IEEE **66**(1), 51–83 (1978).
38. B. Abraham and J. Ledolter, *Statistical Methods for Forecasting* (Wiley, 1983).
39. G. Wilpers, P. See, P. Gill, and A. G. Sinclair, "A monolithic array of three-dimensional ion traps fabricated with conventional semiconductor technology," Nat. Nanotechnol. **7**(9), 572–576 (2012).
40. S. S. Ivanov, N. V. Vitanov, and N. V. Korolkova, "Creation of arbitrary Dicke and NOON states of trapped-ion qubits by global addressing with composite pulses," New J. Phys. **15**(2), 023039 (2013).
41. S. S. Ivanov and N. V. Vitanov, "High-fidelity local addressing of trapped ions and atoms by composite sequences of laser pulses," Opt. Lett. **36**(7), 1275–1277 (2011).

#191977 - $15.00 USD Received 10 Jun 2013; revised 19 Jul 2013; accepted 21 Jul 2013; published 30 Jul 2013

1. Introduction

Coherent control of atomic systems has applications extending to quantum information processing (QIP) of atomic qubits [1], frequency metrology [2], and atom interferometry [3]. Exquisite control of atomic particles' internal and external quantum states by laser radiation has enabled significant progress in these topics. In trapped-ion QIP, agile lasers are used to coherently manipulate the qubit, which may be encoded in electronic ground and metastable excited states via an optical transition [4], or in ground-state hyperfine levels via a Raman transition [5]. In both instances, state-manipulation lasers are required to deliver a sequence of optical pulses tuned to a variety of transitions (eg, carrier, red and blue motional sidebands), with an arbitrary combination of amplitude and phase. These sequences are essential for implementing quantum gates [6,7], algorithms [8,9] and teleportation [10,11] with trapped ions. The same techniques have been employed in quantum metrology with trapped ions [12,13]; the example of quantum logic spectroscopy [14] resulted in optical frequency references at record levels of precision [15]. In optical frequency standards, laser phase agility can be used to create asymmetric optical Ramsey lineshapes [16] suited to oscillator stabilization [17]. A more generalized Ramsey scheme relying on laser pulses that are individually specified in duration, phase and frequency can significantly suppress unwanted systematic shifts in optical atomic clocks [18]. In stimulated Raman cooling of neutral atoms, amplitude and frequency agility of the cooling laser enables sequential interactions with specific velocity classes of atoms, which is required to minimize the ensemble temperature below the photon-recoil limit [19]. Similar control is required for light-pulse atom interferometers as applied to inertial sensing [20–22]. To achieve efficient state transfer via Bragg pulses in large area atom interferometers [23], and realize significantly increased sensitivity, agile frequency and amplitude control of the laser is required [24]. In a neutral-atom cavity QED single-photon source [25], photons can be generated deterministically in arbitrary quantum superpositions of various temporal modes [26]; in that work an agile laser enabled an arbitrary phase change between neighboring time bins within a single photon

All these applications require fast and accurate switching of optical parameters. In the example of trapped ion qubits [6], sequences of multiple pulses must be short compared to the coherence time of the atomic system. Small errors in any parameter of each pulse will reduce the fidelity of logic operations, especially when accumulated over long sequences.

We have developed a laser system which transfers the phase, amplitude and frequency agility, as well as fast switching capability, of a direct digital synthesis (DDS) RF source to a laser beam via acousto-optic modulation. The 674 nm laser system is designed to address the $S_{1/2}$ - $D_{5/2}$ optical qubit transition in $^{88}Sr^{+}$, and is ideal for generating sequences of multiple pulses, including composite pulses [27], with high accuracy. Temporally-profiled optical pulses tailor the excitation laser's Fourier spectrum, thus minimizing the power spectral density in the vicinity of off-resonant transitions, and maximizing quantum gate fidelities. A second acousto-optic modulator permits the generation of a bichromatic laser field for implementing the Mølmer-Sørensen entangling gate [28,29]; this requires frequency components that are tuned close to the red and blue motional sidebands of the qubit carrier transition, which are typically separated by a few MHz.

Previous approaches to laser agility in this context have used separate instruments for the control of AOM frequencies and amplitudes. It is common to use a DDS frequency source together with a variable attenuator [24] or a variable-gain amplifier [30] to determine the amplitude. Another approach uses a mixer to shape the RF signal controlling an AOM [31]. However, little information is presented on specific implementations, appropriate characterization methods and achieved parameters.

In this work we show that a commercial DDS source enables agile control of optical phase, amplitude and frequency from a single instrument, thus simplifying the overall experimental implementation. We achieve agility in optical phase with high precision (≤ 10

#191977 - $15.00 USD Received 10 Jun 2013; revised 19 Jul 2013; accepted 21 Jul 2013; published 30 Jul 2013

mrad) and accuracy (< 0.1%). An automated calibration procedure delivers amplitude-shaped optical pulses, with durations ranging from 500 ns to 500 ms, in near-perfect agreement with the desired functional form. Furthermore, the system exhibits an optical extinction ratio of > 5 × 10^{11}, which is an essential feature for coherent atomic applications. The methods to characterize the optical system accurately and precisely are presented in detail. While this system was developed for $^{88}Sr^{+}$ ions, the general approach is widely applicable to other atomic experiments.

2. Experimental setup

In the context of trapped ions, coherent manipulation of optical qubits requires a frequency-stabilized laser that can be switched in phase, amplitude and frequency with negligible loss of optical coherence. It is also essential to achieve a carrier transition Rabi frequency of up to ~500 kHz; in turn this enables sideband transition Rabi frequencies much greater than the decoherence rates usually encountered in ion traps. Typically, this requires ~2 mW focused to $2w_0$ ~30 μm [16]. In our previous work with $^{88}Sr^{+}$, a frequency-stabilized extended-cavity diode laser (ECDL, 674 nm) of limited power (4 mW) was used [16]. The laser system described here (see schematic in Fig. 1) uses optical injection locking to phase lock a 30 mW laser to the ECDL, permitting multiple AOM passes and fiber coupling to enable fast switching with high extinction, while still providing adequate laser power for driving the $^{88}Sr^{+}$ transition. Furthermore, the AOM enables agility in optical phase (ϕ), amplitude (E) and frequency (ν) without destroying the optical coherence. The principle of this injection-lock approach can be extended to ~1 Hz laser linewidths [32], where coherence times of optical atomic transitions up to ~1 s have been demonstrated [33]. The general setup principles are widely applicable to other systems designed to address transitions in different atomic species.

2.1 Optical layout

The power laser (30 mW) is injected with 1 mW of master laser light via the exit port of a 40 dB optical isolator to produce a robust optical lock. With this approach, the linewidth of the injection-locked laser is only limited by that of the master. A single-mode polarization-maintaining fiber (PMF1, Fig. 1) cleans the mode and decouples the optical alignment between the laser and the AOM setup. AOM1 (at frequency f_1), in double-pass configuration, provides the control of optical ϕ, E, and ν. The return pass light is vertically displaced from the incident beam, and is picked off with a compact mirror. A second modulator (AOM2) in single-pass configuration enables bichromatic operation (at frequencies f_{2A}, f_{2B}). Each AOM runs at ~140 MHz, giving a total frequency shift of ~420 MHz. Light is focused to $2w_0$ = 100 μm inside both AOMs to achieve a measured $1/e^2$ rise time of 30 ns, whilst maintaining a single-pass diffraction efficiency of 80%. Varying f_{2A} changes the diffraction efficiency of AOM2 and the coupling efficiency second PM fiber (PMF2, Fig. 1). When compared to single-frequency operation at 140 MHz, the power out of the second PM fiber is reduced by a 5% (20%) for a bichromatic frequency difference $\delta f_2 = (f_{2A} - f_{2B})$ = 4 MHz (8 MHz). After losses due to modulation and fiber-coupling, up to P_1 = 3 mW can be delivered to the ion; when focused to $2w_0$ = 30 μm, this intensity will meet the Rabi frequency criterion. The low power of the extinguished state (P_2) at the second PM fiber output was measured using a single-photon avalanche photodiode (PerkinElmer SPCM-AQR-14-FC), resulting in an extinction ratio of $P_1/P_2 > 5 \times 10^{11}$. This high level of extinction is essential to minimize unwanted perturbation and subsequent decoherence of the qubit state between programmed excitation pulses.

#191977 - $15.00 USD Received 10 Jun 2013; revised 19 Jul 2013; accepted 21 Jul 2013; published 30 Jul 2013

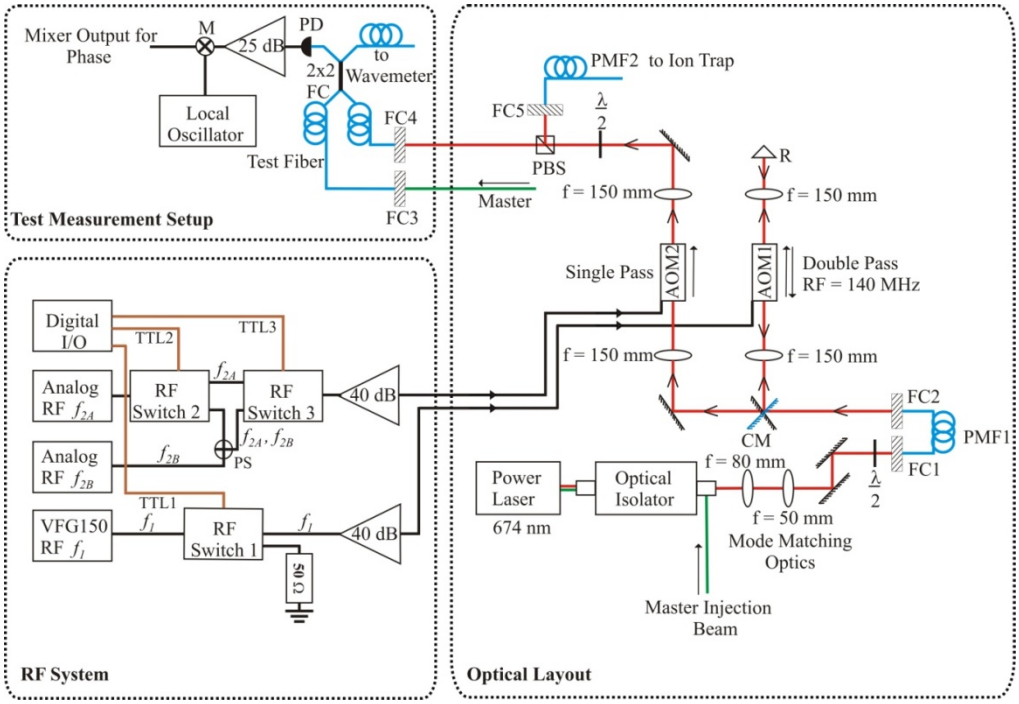

Fig. 1. Schematic of the optical layout, RF system, and test measurement setup. Light from the injection-locked power laser at 674 nm is switched by two AOMs, which also facilitate phase, amplitude and frequency control. The RF system enables agile control of these parameters via a digital synthesizer driving AOM1, as well as the generation of a bichromatic light field via analog synthesizers driving AOM2. The test measurement setup enables routine measurements of the modulated light field. All RF sources are phase locked to a 10 MHz reference signal (not shown). RF switches extinguish signals to the AOMs and change between single-frequency and bichromatic operation. M, RF mixer; PS, RF power splitter; 2 × 2 FC, 2 × 2 fiber coupler; PD, 1 GHz photodiode; FC, fiber collimator; CM, compact mirror; PMF, polarization maintaining fiber; R, right-angled prism (retroreflector).

2.2 RF system

The agility in optical ϕ, E and ν of the system is derived from a single DDS RF source (Toptica Photonics VFG150) which drives AOM1 after amplification. All DDS signal parameters can be switched once every internal clock cycle of 5 ns. The DDS source parameters of phase θ, power P and frequency f_1, can be tuned in the ranges (with resolution): $0 \le \theta < 2\pi$ (< 1 mrad), -54 dBm $\le P \le -4$ dBm (8 bits linear), and 1 MHz $\le f_1 \le$ 150 MHz (< 50 mHz). The 30 ns rise time of AOM1 becomes the limiting factor in the switching speed of all parameters. The DDS output has noise components across its full frequency range, however these are largely filtered by the bandwidth of AOM1. In an optical beatnote spectrum (± 25 MHz range), the largest noise features are at −45 dBc. A high isolation (80 dB) RF switch (Minicircuits ZASWA-2-50DR +) extinguishes f_1 from AOM1 and is controlled by signal TTL1 (see Fig. 1).

As the agility in optical ϕ, E and ν is fully provided by the DDS driving AOM1, analog RF synthesizers are used to drive AOM2 due to their superior noise characteristics. Synthesizers at frequencies f_{2A} and f_{2B} drive AOM2, and are coupled into the same transmission line using a power splitter. Two high isolation RF switches, activated by control signals TTL2 and TTL3, enable three modes of operation: 1) both f_{2A} and f_{2B} are blocked, so AOM2 serves as an optical attenuator, 2) only f_{2A} drives AOM2, giving single-frequency operation, or 3) both f_{2A} and f_{2B} (with δf_2 ~4 MHz) drive AOM2, producing a bichromatic

#191977 - $15.00 USD Received 10 Jun 2013; revised 19 Jul 2013; accepted 21 Jul 2013; published 30 Jul 2013

laser field. Using attenuators, the powers in each input line to RF switch 3 are arranged to ensure that AOM2's diffraction efficiency is identical for operation modes 2 & 3. All RF and digital I/O sources are phase locked to a 10 MHz reference.

2.3 Test measurement setup

Routine measurement of system properties, e.g. noise spectra, optical beatnotes and amplitude-shaped pulses, is enabled by a test setup based on a 2 × 2 fiber coupler and a 1 GHz photodiode (Thorlabs-DET02AFC). Light from before the second PM fiber and a portion of the master injection beam are inputs to the coupler. One output is incident on the photodiode and is used for monitoring power levels and beatnotes; the other is input to a wavemeter. Under typical operating conditions, when AOM1 is supplied with the maximum DDS amplitude, the measured power (P_{meas}) of the modulated light at the test fiber output is P_{max} ~100 μW.

Phase changes are measured by monitoring the 420 MHz beatnote between the light after three AOM passes and the master injection beam. This is demodulated to 1 MHz using a local oscillator at 421 MHz and an RF mixer. The master light is blocked (at FC3, see Fig. 1) when characterizing either the temporal profile of optical pulses or bichromatic operation. Amplitude-shaped pulses are measured directly at the photodiode output; 12-bit measurement resolution was required for enhanced precision. In the case of bichromatic operation, a beatnote at $\delta f_2 = 4$ MHz is detected at the photodiode.

3. System characterization

3.1 Phase agility

Accurate phase control of the optical beam is essential in trapped-ion quantum information [34] where coherent sequences of up to ~30 optical pulses, including composite pulses, are employed [10]. Similarly, spectroscopic measurements using optical Ramsey [16,35] and hyper-Ramsey [18] techniques also rely on accurate phase control. In these applications, any inaccuracies in implementing phase steps will accumulate over the sequence and lead to decreased coherence times.

A programmed phase shift $\delta\phi = (\phi_1 - \phi_2) = \pi$ in the 1 MHz demodulated signal, as described in section 2.3, is shown in Fig. 2(a). The timing of the phase step can be controlled with 5 ns resolution, and accuracy only limited by the 10 MHz reference stability. Sinusoidal fits to the 1 MHz signal are taken either side of the phase step using the Levenberg–Marquardt (L-M) fitting algorithm [36] to calculate the measured phase step value, using only δϕ and amplitude as fitting parameters. The central 1 μs of the trace is ignored in the fitting procedure as the signal is non-sinusoidal in a short period after the phase shift. In Fig. 2(b), the fit to the data before the phase change is extended in duration, and shifted by π at the programmed switching time. The extended function converges to the data after ~200 ns, which is determined by the AOM's 30 ns rise time and the non-linearity of the mixer; the latter feature was determined by an independent RF measurement.

#191977 - $15.00 USD Received 10 Jun 2013; revised 19 Jul 2013; accepted 21 Jul 2013; published 30 Jul 2013

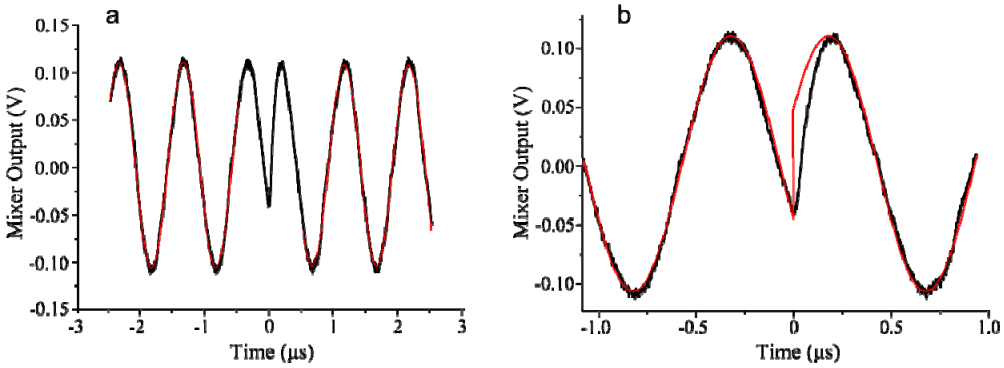

Fig. 2. A single-shot measurement of a phase step $\delta\phi = \pi$. (a) Two fits (red) to the data (black), on either side of the phase step, are used to calculate $\delta\phi$. The central 1 μs of the trace is ignored in the fitting procedure. (b) A zoomed-in version of the same data (black) with the fit from before the phase step extended throughout (red), including $\delta\phi = \pi$ at the programmed switching time ($t = 0$).

The average of 25 single-shot phase shift measurements is plotted against the programmed value, and repeated over the range $0 \leq \delta\phi \leq 2\pi$, as shown in Fig. 3(a). A linear fit yields a gradient of 1.00086(2), showing accurate phase control over the full range. Figure 3(b) shows a higher resolution measurement, where the average of 45 single-shot measurements per programmed value is plotted in increments of 10 mrad, and the fitted gradient is 1.000(5). In both Figs. the error bars are shown as the standard deviation of the mean. Amplification noise in the demodulated signal (at ~4.5% of the peak to peak signal) prevents phase steps at the limit of resolution of the DDS (< 0.1 mrad) from being resolved in the measurement.

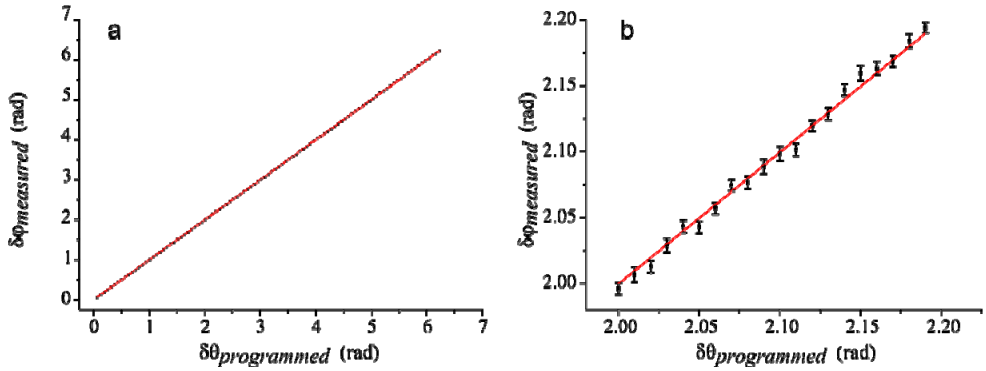

Fig. 3. (a) Measured phase change ($\delta\phi_{measured}$) as a function of the programmed value ($\delta\theta_{programmed}$) from 0 to 2π rad in increments of π/50 rad, where each data point is the average of 25 single-shot measurements. The fitted gradient is 1.00086(2), indicating accurate phase control over the full range. The error bars are smaller than the data points in this plot. (b) A higher resolution measurement, in increments of 10 mrad, with each data point representing the average of 45 single-shot measurements. The fitted gradient is 1.000(5), indicating accurate control at this fine resolution.

3.2 Amplitude calibration and agility

By controlling the temporal profile of an optical pulse's amplitude, the power spectral density remote from the carrier frequency can be greatly suppressed when compared to the case of a square pulse. The Blackman function is a favored form due to its high side lobe suppression under a Fourier transform; other related functions perform a similar role [37]. In coherent interactions with atomic systems, this reduces unwanted off-resonant excitation of nearby transitions. When addressing a weaker motional sideband transition of a trapped ion,

#191977 - $15.00 USD Received 10 Jun 2013; revised 19 Jul 2013; accepted 21 Jul 2013; published 30 Jul 2013

minimizing the interaction with the stronger off-resonant carrier is crucial to maximizing coherence of the operation. Amplitude-shaped optical pulses were critical in a two qubit trapped-ion entangling gate of record fidelity [29]. Blackman pulse shapes were essential for addressing atoms with a specified velocity distribution in stimulated Raman cooling [19]. Gaussian temporal profiles of optical pulses were used to create a large momentum splitting of the paths in atom interferometers [23].

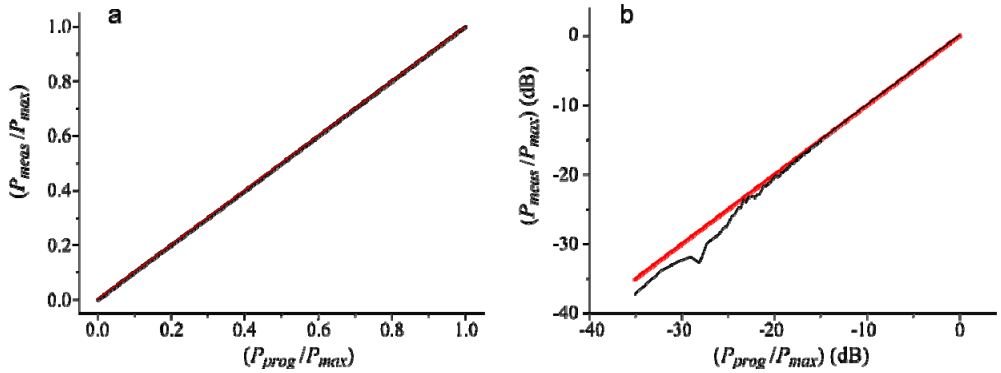

Fig. 4. After the calibration routine to compensate for non-linear response of the AOM, the optical power from the test fiber output (P_{meas}) was measured as a function of the programmed optical power (P_{prog}). Both powers were scaled to the maximum power available from the test fiber (P_{max}), and the measured waveform consists of 3236 samples. (a) The linear fit (red) to the data (black) yields a gradient of 0.99938(2). (b) The same data and fit are presented in a log-log plot, showing that deviation from linear behavior is only significant at powers at least 20 dB below the peak power.

To account for the non-linear optical response of AOM1, and enable production of optical pulses with arbitrary shape, an automated calibration routine was developed. This sets the DDS RF amplitude via USB and records the photodiode signal with a 14-bit digitizer. Firstly, optical power is recorded at the test fiber output as a function of the DDS RF amplitude, and averaged over 200 such measurements to evaluate the AOM's response. A 9th order polynomial fits the data well, since the associated residuals exhibit no modulation, and acts as a calibration function to specify the DDS amplitude for a desired optical power. To verify the calibration, a 4 ms linear ramp in programmed optical power (P_{prog}) from 0 to P_{max} is recorded; see Fig. 4(a). Figure 4(b) shows the same data and fit on a logarithmic scale. The ratio of optical powers out of the test and second PM fibers can be used to specify an arbitrary power (up to 3 mW) delivered to the ion trap via the latter fiber. The procedure's duration is < 5 s, enabling small alignment drifts to be accounted for intermittently.

The calibrated system can produce amplitude-shaped pulses, suitable for atomic excitation schemes, with high accuracy. A Blackman pulse of duration $2T$ and amplitude E_0 has a profile of the form [37]

$$E(t)=\begin{cases} E_0\left[0.42-0.5\cos\left(\pi t/T\right)+0.08\cos\left(2\pi t/T\right)\right] & \text{for } 0\le t\le 2T \\ 0 & \text{elsewhere} \end{cases}. \quad (1)$$

To create an optical pulse with electric field amplitude $E(t)$, the system is programmed to generate a pulse of the form $E^2(t)$ in power. The data in Fig. 5(a) shows a measurement of a Blackman pulse of 500 μs duration, fitted to $E^2(t)$ with the L-M algorithm, using only E_0 as a free parameter. Figure 5(b) shows the same data on a logarithmic scale; the deviation from the ideal form near the noise floor of the measurement is clear. This is expected from the deviation of the fit and data at low optical powers in Fig. 4(b).

#191977 - $15.00 USD Received 10 Jun 2013; revised 19 Jul 2013; accepted 21 Jul 2013; published 30 Jul 2013

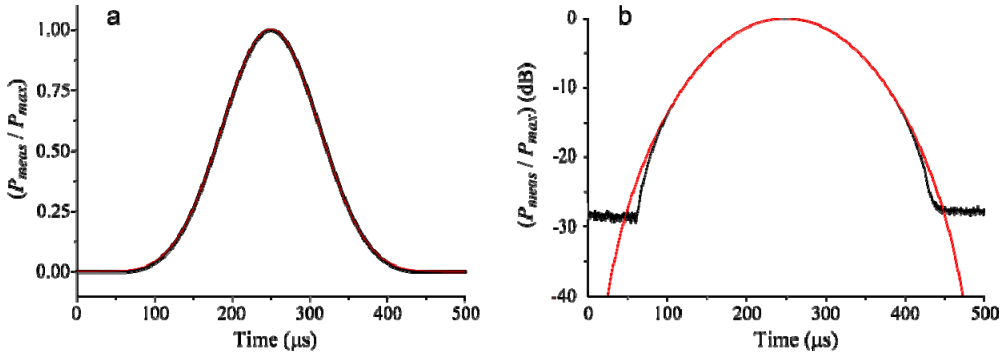

Fig. 5. Data (black, average of 200 single-shot measurements) and fit (red) of a measured Blackman pulse of duration $2T$ = 500 μs. The data points are recorded at intervals of 0.224 μs and the fit is of the form $E^2(t)$ (see Eq. (1)). The optical power recorded from the test fiber output (P_{meas}) is scaled to the maximum power available (P_{max} = 100 μW). The data and fits are plotted with the measured power axis on (a) a linear, and (b) a logarithmic scale. The latter shows the fit deviates from the data at low powers and settles completely at the noise floor of the measurement.

The coefficient of determination (*COD*) indicates quantitatively how much of the deviation in the data about the mean is attributable to the fitted model [38], with *COD* = 1 indicating a perfect fit of all data points. The fit of Fig. 5(a) gives *COD* > 0.99995, demonstrating a close agreement between the data and the ideal $E^2(t)$ form. Blackman pulses can be produced accurately over six orders of magnitude in duration, as shown in Fig. 6(a)-6(d), where each fit to $E^2(t)$ has a *COD* > 0.99992. The excellent match of a pulse's measured shape to the programmed form is limited by AOM1 at very short times by the AOM rise time, and at durations of a few seconds by alignment drift due to thermal effects.

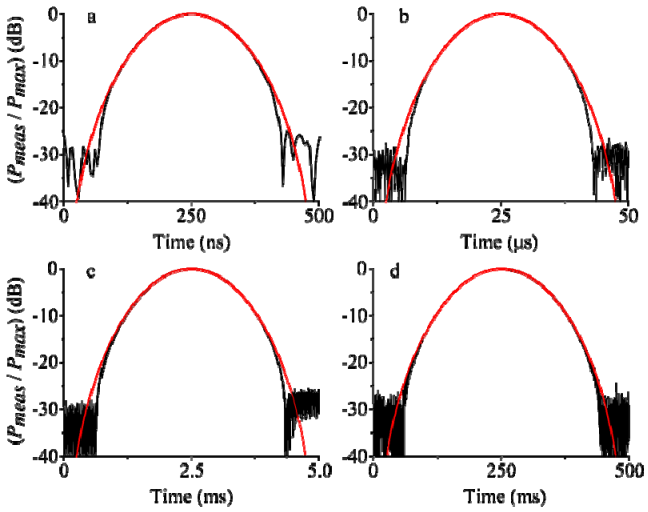

Fig. 6. Accurate Blackman pulse shapes are produced with durations varying over six orders of magnitude: (a) 500 ns, (b) 50 μs, (c) 5 ms and (d) 500 ms. The *COD* fitting parameter is > 0.99992 for each. To record (a), it was necessary to increase the optical power to P_{max} = 1 mW.

A more stringent test of calibration procedure accuracy is to calculate the discrete Fourier transform (DFT) of the measured pulse shape. A programmed Blackman pulse of duration $2T$ = 500 μs, as shown in Fig. 5(a), was measured over 200 single shots and averaged to reduce measurement noise. The resulting data was processed by the DFT algorithm, as shown in Fig. 7. For comparison, the DFT was calculated for a measured square pulse containing the same integrated power as the Blackman pulse of Fig. 5(a), as well as for the simulated function

#191977 - $15.00 USD Received 10 Jun 2013; revised 19 Jul 2013; accepted 21 Jul 2013; published 30 Jul 2013

$E^2(t)$ with $2T = 500$ μs. In the range where the Fourier frequency is greater than $100/2T = 200$ kHz, the power spectral density of the Blackman pulse is ~27 dB below that of the square pulse. This difference demonstrates the advantage of using amplitude-shaped pulses for coherent excitation experiments. The discrepancy between data and theory for the Blackman pulse (beyond $20/2T$ = 40 kHz) is mainly due to the noise floor of the averaged data, measured at −48 dBc. We considered the effect of this reduction in the instance of trapped ions, when resonantly driving a π-pulse on a blue motional sideband transition in a typical experiment. The sideband's parent carrier, detuned by the ion's motional frequency, is the closest strong transition which can be driven off-resonantly. By choosing the pulse's Fourier-transform linewidth to be < 0.1 of this detuning, the power spectral density resonant with the carrier is close to the measurement noise floor. Taking this as an upper limit, we estimate a 2% reduction in the fidelity of the operation. If the spectral density was at −60 dBc, this infidelity would reduce to 0.2%, below the level of other dominant sources of decoherence.

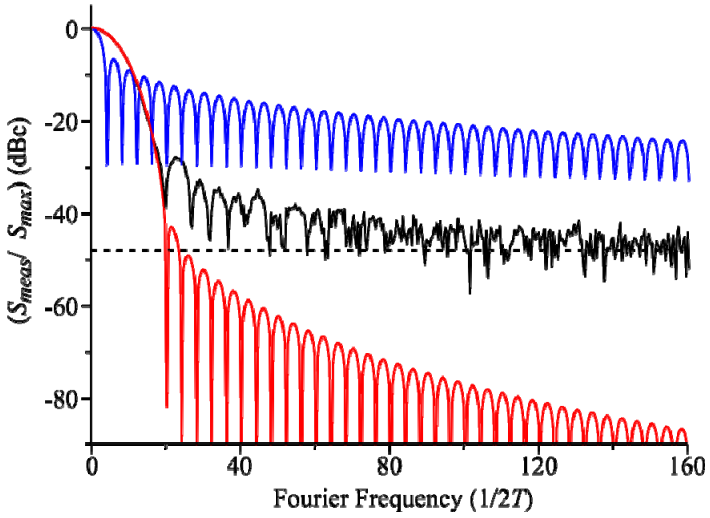

Fig. 7. The power spectral density distribution of measured optical pulse shapes as determined by a discrete Fourier transform (DFT). A Blackman pulse of duration $2T = 500$ μs (black) is compared to a square pulse (blue) of the same duration and the same integrated optical power. The measured power spectral density (S_{meas}) is quantified with respect to the carrier maximum (S_{max}). The Blackman pulse exhibits a substantial reduction in S_{meas}/S_{max} at the higher Fourier frequencies as expected; quantifying this reduction is limited by the measurement noise floor (independently determined to be –48 dBc, as shown by the dashed line). The DFT of the fit to the Blackman pulse in Fig. 5 is also presented (red) and shows a close match to the DFT of measured pulse above the measurement noise floor. For each DFT, the sample interval was 16 ns and the sample length was 312,505.

3.3 Frequency agility

For coherent control of trapped ions, extensive pulse sequences may address different transitions consecutively, necessitating frequency switching on a timescale much less than the gate operation time. The system developed here enables arbitrary sequences of single-frequency or bichromatic pulses; the latter feature is required for the Mølmer-Sørensen entangling gate operation [29]. Moreover, the double-pass AOM permits the optical frequency to be tuned to the carrier and sidebands of different Zeeman components in the $^{88}Sr^{+}$ $S_{1/2}$ - $D_{5/2}$ spectrum. When AOM1 is optimized for maximum diffraction efficiency at f_1 = 140 MHz, tuning f_1 by ± 5 MHz (± 10 MHz) reduces the power transmitted from the second PM fiber by 5% (9%). In the application of trapped ions, this small variation will be accounted for when the Rabi frequencies of the laser on different transitions are routinely

#191977 - $15.00 USD Received 10 Jun 2013; revised 19 Jul 2013; accepted 21 Jul 2013; published 30 Jul 2013

measured. Alternatively, this reduction could be calibrated and then compensated for by a programmed increase in RF power to AOM1.

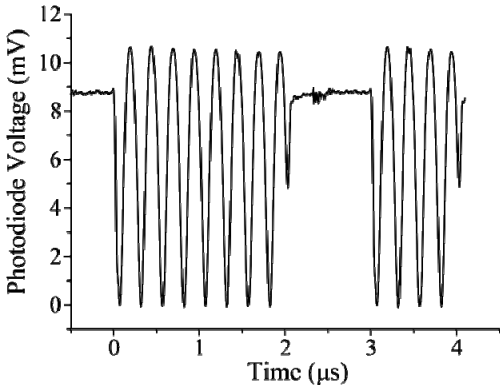

Fig. 8. Switching between single-frequency and bichromatic modes of operation. A 4 MHz beat signal is observed when the system is in bichromatic mode, activated by control signals TTL2 and TTL3. The displayed signal is the average of 39 single-shot measurements. The noise features (at 1.4, 2.4 and 3.4 μs) are due to pick up of the TTL control signal in the measurement process.

In bichromatic mode, AOM2 is driven with f_{2A} = 138 MHz and f_{2B} = 142 MHz so that the optical beam carries two frequencies, separated by twice the axial trapping frequency of the ion (~2 MHz in typical experiments [4,39]) as required in the Mølmer-Sørensen scheme [29]. In single-frequency mode only f_{2A} drives AOM2. To demonstrate fast switching between modes, changes between bichromatic and single-frequency operation are measured. In bichromatic mode, a 4 MHz beatnote is detected at the photodiode (see Fig. 1), whereas in single-frequency mode only a d.c. voltage is detected. Figure 8 shows an example sequence, with 2 μs of a 4 MHz beat, followed by 1 μs of single-frequency operation, followed by 1 μs of the 4 MHz beat. Control signals TTL2 and TTL3 are derived from a digital I/O source that shares the same 10 MHz reference as all RF sources, enabling precise control of the number of beat periods in a bichromatic pulse.

4. Conclusions

We have constructed and characterized a 674 nm laser system that is fully agile in phase, amplitude and frequency for the purpose of coherent optical interactions with trapped $^{88}Sr^{+}$ ions. Measurements demonstrate that the agility of a DDS RF source is transferred to the optical beam via an AOM with high precision and accuracy. The phase of the optical beam can be switched in ~30 ns with a measurable resolution of 10 mrad and accuracy better than 0.1%. An automated procedure calibrates the non-linear response of the RF and AOM system, which enables amplitude-shaped pulses of arbitrary shape and duration to be produced. In turn, this facilitates tailoring of an optical pulse's Fourier spectrum; comparing the DFT of measured Blackman and square pulses demonstrates the significant reduction of spectral density at Fourier frequencies remote from the carrier in the former. Blackman pulses with durations ranging over six orders of magnitude from 500 ns to 500 ms, in near-perfect agreement with the desired functional form, have been demonstrated. The optical system is configured to permit switching between single-frequency and bichromatic operation on sub-microsecond timescales, for the purpose of implementing the Mølmer-Sørensen entangling gate operation in $^{88}Sr^{+}$. Additionally, switching of optical pulses is achieved with a high extinction ratio of $> 5 \times 10^{11}$, which is an essential feature for maintaining atomic coherence in the "absence" of light during pulse sequences.

The principles of the system described here are readily transferable to different laser wavelengths for coherent manipulation of other ion species with extensive pulse sequences. In

#191977 - $15.00 USD Received 10 Jun 2013; revised 19 Jul 2013; accepted 21 Jul 2013; published 30 Jul 2013

respect of trapped ions, the techniques presented are highly relevant to applications in quantum information processing and precision quantum metrology. The approach described here is suited to applications where accurate and high resolution phase control is required; for example, in recent proposals for generating Dicke and N00N states in trapped ions [40], as well as for high-fidelity local addressing of trapped atoms/ions by composite sequences of laser pulses [41]. Beyond ions, the general principles are also relevant to neutral atom systems used in quantum information with cavity QED [26], and atom interferometry for precision inertial sensing [20–22].

Acknowledgments

This work was supported by the UK's National Measurement Office EMT research programme, and EPSRC through the Doctoral Training Centre in Optics and Photonics Technologies. We thank D. Humphreys and P. Harris for helpful discussions.

#191977 - $15.00 USD Received 10 Jun 2013; revised 19 Jul 2013; accepted 21 Jul 2013; published 30 Jul 2013